CHALMERS

Layered solid-shell elements for accurate prediction of stresses in laminated composites

Master's thesis in Applied Mechanics

ELIAS BÖRJESSON

MASTER'S THESIS IN APPLIED MECHANICS

Layered solid-shell elements for accurate prediction of stresses in laminated composites

ELIAS BÖRJESSON

Department of Applied Mechanics
Division of Solid Mechanics
CHALMERS UNIVERSITY OF TECHNOLOGY

Göteborg, Sweden 2016

Layered solid-shell elements for accurate prediction of stresses in laminated composites
ELIAS BÖRJESSON

Cover:
White color.

Layered solid-shell elements for accurate prediction of stresses in laminated composites
Master's thesis in Applied Mechanics
ELIAS BÖRJESSON
Department of Applied Mechanics
Division of Solid Mechanics
Chalmers University of Technology

Abstract

Laminated composite materials possess very good weight to strength properties, and are therefore desirable in a wide range of engineering applications. Light-weight composites have traditionally only been used in the marine- and aero-industry due to expensive and time consuming manufacturing processes, but is now also being considered as a viable option within the automotive-industry. The introduction of layered composites does, however, present new CAE challenges. For example, complex failure mechanisms such as delamination and crack propagation are driven by the transverse stresses in the material, and are difficult to capture efficiently using standard modeling techniques. The aim of this thesis is therefore to develop a solid-shell element with increased capability (compared to Mindlin type shells) of predicting the transverse stress components through the laminate.

The solid-shell element developed is based on a traditional eight node solid element (brick element). In order the prevent various locking phenomenas, the compatible strain field is enhanced using a combination of the Enhanced Assumed Strain (EAS) and the Assumed Natural Strain (ANS) methods. The element is shown to produce accurate and efficient out-of-plane bending results, when applied to analysis of thin plate and curved structure problems.

Three approaches to improve the accuracy of the transverse stresses in the solid-shell elements, have been studied in this thesis. The first approach is based on a three field variational formulation and assumes a higher order variation of the transverse stresses. Unfortunately, poor results in the predicted stresses were obtained. The second approach predicts the transverse stresses, by recovering them using the equilibrium equations, in a post processing step. This method is shown to accurately and efficiently predict the full 3D stress field in thin plate analyses. The third and last approach, obtains the complete stress field by using multiple solid-shell elements through the thickness of the composite material. Also this approach produces accurate stress predictions; however, it is computationally expensive since a relatively fine discretization is needed.

Keywords: Solid-shell, Laminated composites, Transverse stresses, Stress Recovery, FEM

Preface

This work is the concluding part of my master studies in Applied Mechanics at Chalmers University of Technology. It was performed during the spring of 2016. I would like to thank my supervisor, Jim Brouzoulis, for always being able to help me and give me feedback on my work.

Elias Börjesson, 2016

Contents

1   Introduction

The increasing demand for lighter and stronger structures, have made composite materials a vital tool for today's engineers. Composites can now be found in a wide range of applications, e.g. in the automotive industry and in aero space structures [15, 3]. The advantage of composites comes from its ability to be customized for a specific application, thereby reducing superfluous strength and weight. For the vehicle industry, the benefits of this are clear; lower weights means less fuel consumption, which ultimately leads to a decreased impact on the environment.

There are several different types of laminated composites, some common are

- **Unidirectional fiber composites**. Materials with long fibres oriented in one direction, which are held together by a matrix material. This leads to a large strength in the longitudinal direction of the fibers, but reduced strength in the transverse direction.

- **Woven fiber composites**. This composite is similar to unidirectional fiber composites, however the fibres are woven together. This leads to similar strength in all directions in the plane, however the material demonstrates weaker response in compression due to waviness in the fibers.

- **Sandwich constructions**. Layered structures consisting of a lightweight core material of relatively low strength, bounded by two thin and stiff skins on each side. The core material provides a high bending stiffness with overall low density.

The introduction of new complex composite structures does however present great challenges. Layered composites demonstrate complex failure mechanisms not experienced by traditional homogeneous materials, and are therefore difficult to capture with current modeling techniques. Two such mechanisms are inter- and intralaminar cracking which greatly affects the structural response, and therefore needs to be modeled. In many industrial applications, it is not feasible to explicitly model these cracks with finite elements, because the computational cost would be too great, even for the computers of today. Instead, new possibilities in efficient FE-modeling of composites needs to be researched.

The underlying cause behind crack initiations and crack propagation, are the transverse stresses experienced by the material. It is therefore of great interest to be able to determine the complete stress state in composites. Most of today's composite modeling techniques, based on shell-kinematics or high resolution meshes (with solid elements), lack the ability to capture the complete stress state, or, requires a substantial amount of computer resources to do so. Much effort in the scientific community is therefore put on developing new methods for stress prediction in composites.

Due to the limitations of today's standard modeling techniques, this project seeks to develop an eight node solid-shell element, with increased capabilities of accurately predicting all stress components in a layered composite. The solid-shell will be based on a standard eight node brick element. However, as well documented in the literature, traditional brick elements experience many different types of locking behaviors when analysing thin structural components. Furthermore, low order brick elements lacks the kinematic freedom to accurately represent the transverse stress components in a material. Therefore, a large focus on addressing these problems is made in this project.

1.1   Concepts and issues in modeling of laminated composites

This section gives the reader an overview of important concepts and common challenges when modeling layered composites. As mentioned in the section above, a great challenge is to efficiently predict the transverse stress components within the material. The in-plane stresses in a laminated structure, are in general discontinuous through the thickness. On the other hand, the transverse stresses are always

continuous through the thickness of the material [3]. This can be seen from Newtons third law, where the forces acting on the top of one lamina, must be equal to the force acting on the bottom surface of the adjacent lamina. This fact is referred to in the literature as interlaminar continuity (IC) of transverse stresses. Figure 1.1a and 1.1b shows a schematic view on how the in-plane and transverse stresses can vary through the thickness in a layered composite.

A second important fact to consider, is that the mechanical properties within a composite may be discontinuous and inhomogeneous, due to the stacking of plies of different materials and/or orientations. These transverse discontinuities, causes the displacement fields in the thickness direction to change rapidly between layers. A schematic representation of this is illustrated in Figure 1.1c. This effect is a unique for layered structures, and is known as the zig-zag (ZZ) form of displacement fields in the thickness direction. For an extensive review of the zig-zag effect, and development ideas to capture this behaviour, see the summary by Carrera [3].

Classical theories originally developed for isotropic single-layer structures, such as Kirchhoff and Mindlin-Reissner plate theories, have been extended for modeling of composites. These theories utilizes plane stress assumptions, which is not always suitable for layered composites, since important information about the transverse stresses are lost. Furthermore, laminated composites does in general demonstrate anisotropic material behaviour with large ratios in mechanical stiffness properties ($E_L/E_z \approx 5 \sim 40$, i.e stiffness ratio between length and thickness directions is large). This means that the transverse effects have a much larger influence on the solution (compared to isotropic material cases) [3], making the plane stress assumption even more inapplicable.

Nevertheless, composite modeling techniques based on Mindlin-Reissner theory are still able to accurately predict global characteristics such as deflection and in-plane stresses. In this approach, the plies in the composite are homogenized through the thickness, and is therefore referred to as an equivalent single layer model (ESL). These models are usually adequate for describing the behavior of thin composite shells, however, they typically fail to accurately model moderately thick laminates [7]. As stated earlier, the transverse stresses predicted by ESL models are generally poor or non-existent.

A second common approach for modeling layered structures, is to use so-called layer-wise models (LW). This means that a separate displacement field expansion is assumed within each layer. Moreover, some LW-models ensure that the transverse stress components are compatible between layers [3]. The direct benefits with this approach is that it is possible to capture the full three-dimensional stress field, and fulfil IC and ZZ, which is not possible in traditional ESL models. However, LW models leads to a large number of degree of freedom, drastically increasing the computational cost. Careful consideration is therefore needed if information about transverse affects are important (LW), or if in-plane information are adequate (ESL).

(a) *In-plane stresses*   (b) *Transverse stresses*   (c) *Displacements*
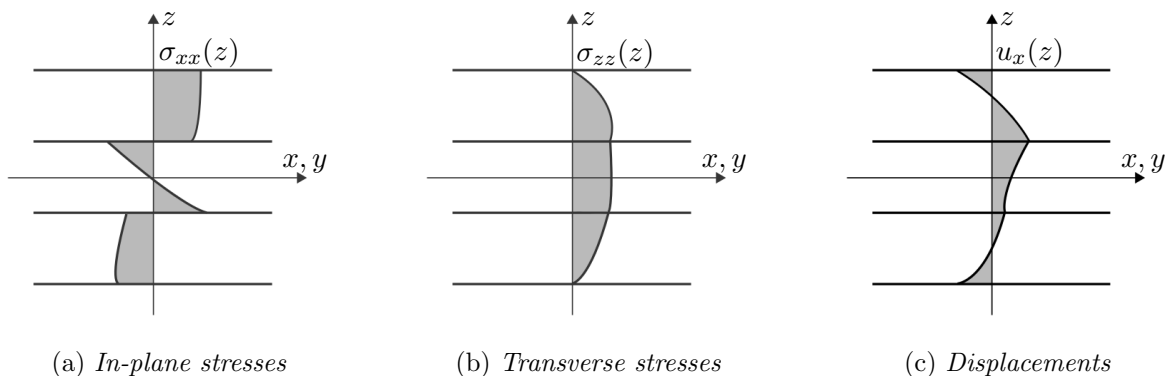
Figure 1.1: *Examples of how the in-plane stresses, out-of-plane stresses and displacements vary through the thickness for a laminate. The displacements and out-of-plane stresses are continuous over the interfaces while the in-plane stresses are discontinuous.*

2 Layered solid-shell element

In this thesis, a solid-shell element refers to a solid continuum element with no rotational degrees of freedom, and possess shell-like qualities. Solid-shell elements have some benefits over traditional shells, to be more suited for three dimensional loading cases (due to an actuall thickness direction), and easier stacking capabilities (placing elements on top of each other). They are also useful for modeling shell-like portions of 3D structures without the need to connect solid element degrees of freedom (translational) to shell degrees of freedom (rotational and translational).

2.1 General kinematics for the solid-shell element

Figure 2.1 shows a solid-shell element in the parent domain, where ξ, η, and ζ are natural coordinates ranging from $[-1, 1]$. The element's initial configuration, $\boldsymbol{X}$, current configuration, $\boldsymbol{x}$, and displacement, $\boldsymbol{u}$, can be represented in a isoparametric fashion as

$$\boldsymbol{X}(\xi,\eta,\zeta) = \sum_{i=1}^{N^u} N_i(\xi,\eta,\zeta)\hat{\boldsymbol{X}}_i, \qquad \boldsymbol{u}(\xi,\eta,\zeta) = \sum_{i=1}^{N^u} N_i(\xi,\eta,\zeta)\hat{\boldsymbol{u}}_i, \qquad \boldsymbol{x}(\xi,\eta,\zeta) = \boldsymbol{X} + \boldsymbol{u} \qquad (2.1)$$

where $N_i(\xi,\eta,\zeta)$ is shapefunction i of the element, $\hat{\boldsymbol{X}}_i$ and $\hat{\boldsymbol{u}}_i$ are nodal coordinates and displacements of the element, respectively, and N^u is the number of nodes in the element. Note that this is the same formulation as for standard solid/brick-elements.

By restricting the element to an hexahedron with only eight nodes, the common thick-shell assumption is obtained, i.e normals to the mid-surface are assumed to stay straight during deformation. The eight trilinear shapefunctions, N_i, are then expressed as

$$N_i(\xi,\eta,\zeta) = \frac{1}{8}\left(1+\xi\xi_i\right)\left(1+\eta\eta_i\right)\left(1+\zeta\zeta_i\right), \quad i = 1,2,\ldots,8 \qquad (2.2)$$

The variables ξ_i, η_i and ζ_i are the parent corner-coordinates for the element in Figure 2.1. An alternative way of representing the solid-shell configurations [20, 18], is as follows,

$$\boldsymbol{X}(\xi,\eta,\zeta) = \frac{1}{2}(1+\zeta)\boldsymbol{X}_{\mathrm{T}}(\xi,\eta) + \frac{1}{2}(1-\zeta)\boldsymbol{X}_{\mathrm{B}}(\xi,\eta) \qquad (2.3)$$

where subscripts T and B denote the top and bottom surfaces, respectively. This formulation is equivalent to that in Equation (2.1) in combination with Equation (2.2), however, defines ζ as the preferred thickness direction.

Beyond the kinematic formulation presented in this section, solid-shell elements need to be able to represent complete tri-linear strains [19]. Without this property, they will not be appropriate for modeling thin structural components. The reason for this is explained in Section 2.3.
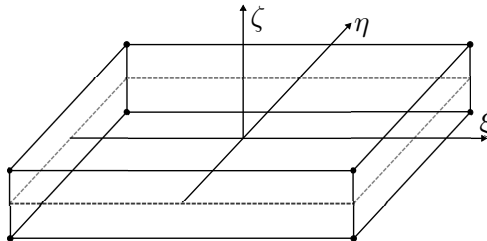
Figure 2.1: *A solid element in parent domain.*

3

2.2 Governing equations for solid-shell element

Two governing equations for a continuum solid will be used in this project. For simplicity, we restrict the study to linear elastic material behaviour.

The principle of minimum potential energy

The well known principle of minimum potential energy is defined as

$$\Pi_{\mathrm{P}} = \int_V W \, \mathrm{d}V - \int_V \boldsymbol{b} \cdot \boldsymbol{u} \, \mathrm{d}V - \int_S \boldsymbol{t} \cdot \boldsymbol{u} \, \mathrm{d}S \tag{2.4}$$

where $\boldsymbol{b}$ is the body forces in a domain V, $\boldsymbol{t}$ is the traction on a surface S and $\boldsymbol{u}$ is the unknown displacement field. W denotes the stored energy function, and can be calculated as

$$W = \frac{1}{2}\boldsymbol{\varepsilon} : \mathbf{D} : \boldsymbol{\varepsilon} \tag{2.5}$$

where $\mathbf{D}$ is the forth order elastic stiffness tensor of the material, and $\boldsymbol{\varepsilon}$ is a strain field.

The Hu-Washizu principle

The variational principle of Hu-Washizu (HW)[1] is defined by the functional [17]

$$\Pi_{\mathrm{HW}} = \int_V W - \boldsymbol{\sigma} : (\boldsymbol{\varepsilon}^u(\boldsymbol{u}) - \boldsymbol{\varepsilon}) \, \mathrm{d}V - \int_V \boldsymbol{b} \cdot \boldsymbol{u} \, \mathrm{d}V - \int_S \boldsymbol{t} \cdot \boldsymbol{u} \, \mathrm{d}S \tag{2.6}$$

where $\boldsymbol{\varepsilon}^u$ is the compatible strain field (dependent on the displacement field), $\boldsymbol{\varepsilon}$ is a independent (unknown) strain field, and $\boldsymbol{\sigma}$ is the stress field,

$$\boldsymbol{\varepsilon}^u(\boldsymbol{u}) = \frac{1}{2} \left(\boldsymbol{\nabla} \otimes \boldsymbol{u} \right)^{\mathrm{sym}}, \quad \boldsymbol{\sigma} = \mathbf{D} : \boldsymbol{\varepsilon} \tag{2.7}$$

HW is derived from the principle of minimum potential energy, see [10] for more information.

2.3 Locking phenomenas in FE-elements

Locking is a term describing the overestimation of the stiffness in a structure or element, leading to poor prediction of the structural response. Solid elements with linear interpolation, as in Equation (2.2), are especially susceptible to many locking phenomenas. Special precautions to remedy these problems are therefore needed in order to obtain an element that is usable in analysis of shell like structures. Below, some common locking phenomenas are described.

Volumetric locking. The so called volumetric locking effect, is the inability of elements to deal with incompressible material behaviours (often encountered in rubber elasticity and metal plasticity) [11]. Simply put, for incompressible materials Poisson's ratio will go towards 0.5, resulting in the bulk modulus approaching infinity, which causes a singular stiffness matrix.

Poisson/thickness locking. This locking phenomena occurs in out-of-plane bending analyses using solid elements. The underlying reason for this effect is the approximation on the displacement field. A linear displacement approximation, will produce constant transverse normal strains through the thickness, which will couple with the linearly varying in-plane strains due to the Poisson's effect. This causes a discrepancy between the transverse and in-plane strains, leading to overestimation of the stiffness [11].

---

[1]Many articles refer to HW as a three field variational [18, 19], however in [10] it is shown that HW is a two field variational formulation.

Shear locking. Shear locking can be found in for example eight node solid elements and bilinear Mindlin plate elements. The effect can be seen when considering a plate subjected to pure bending, for which the out-of-plane shear stresses should be zero. However, the transverse shear strains cannot vanish at all points within the element when it is subjected to pure bending, due to the linear approximation of the out-of-plane displacements [4]. This causes the stiffness of the element to be overestimated.

Trapezoidal/curvature locking The trapezoidal locking effect occurs when, for example, solid element takes a trapezoidal shaped form, i.e the element edges in the thickness direction is not perpendicular to the mid-surface [11]. The trapezoidal shape (that is unavoidable when modeling curved structures), activates incompatible normal strains in the thickness direction, which may cause the locking [8]. These shapes are unavoidable when modeling curved structures.

Membrane locking. Membrane locking describes curved element's inability to exactly represent pure bending deformations. This locking effect is seldom found in linear elements, while quadratic elements show strong membrane locking. The membrane locking problem becomes more pronounced as the thickness decreases [11].

The unwanted locking behavior in FE-elements has led to a lot of research in this area. Two effective methods for eliminating or reducing locking behaviors are the Enhanced Assumed Strains (EAS) method and Assumed Natural Strains (ANS) method. These are described below.

2.4 Enhanced Assumed Strains

The EAS method was first proposed by Simo and Rifai [23], and is an effective method for eliminating some of the locking phenomenas described above. The key assumption in the method is the enhancement of the strain field

$$\boldsymbol{\varepsilon} = \boldsymbol{\varepsilon}^u(\boldsymbol{u}) + \boldsymbol{\varepsilon}^{\mathrm{A}}(\underline{\alpha}) \tag{2.8}$$

where $\boldsymbol{\varepsilon}^u$ and $\boldsymbol{\varepsilon}^A$ are the compatible and enhanced strain fields, respectively, and $\underline{\alpha}$ is a vector of parameters representing the enhanced strain field. The EAS method emanates from the HW functional in Equation (2.6). Using HW together with Equation (2.8), and taking the first variation $\delta\Pi_{\mathrm{HW}}$, leads to the following three equations

$$\int_V \delta\boldsymbol{\varepsilon}^{\mathrm{A}} : (\boldsymbol{\sigma}^\varepsilon - \boldsymbol{\sigma})\,\mathrm{d}V = 0 \qquad\qquad \forall\delta\boldsymbol{\varepsilon}^{\mathrm{A}} \in \mathbb{E}$$

$$\int_V \delta\boldsymbol{\sigma} : \boldsymbol{\varepsilon}^{\mathrm{A}}\,\mathrm{d}V = 0 \qquad\qquad \forall\delta\boldsymbol{\sigma} \in \mathbb{S} \qquad (2.9)$$

$$\int_V \delta\boldsymbol{\varepsilon}^u : \boldsymbol{\sigma}^\varepsilon\,\mathrm{d}V - \int_V \delta\boldsymbol{u}\cdot\boldsymbol{b}\,\mathrm{d}V - \int_\Gamma \delta\boldsymbol{u}\cdot\boldsymbol{t}\,\mathrm{d}V = 0 \qquad\qquad \forall\delta\boldsymbol{u} \in \mathbb{U}^0$$

where $\boldsymbol{\sigma}^\varepsilon = \frac{\partial}{\partial\boldsymbol{\varepsilon}} W(\boldsymbol{x}, \boldsymbol{\varepsilon}^u + \boldsymbol{\varepsilon}^{\mathrm{A}}) = \mathbf{D} : \boldsymbol{\varepsilon}$, and where the following spaces have been introduced

$$\mathbb{U}^0 = \left\{ \boldsymbol{u} \in \mathbb{H}^1(V) \quad | \quad \boldsymbol{u} = 0 \text{ on } \Gamma_D \right\} \tag{2.10}$$

$$\mathbb{E} = \{ \boldsymbol{e} \in \mathbb{L}_2(V) \} \tag{2.11}$$

$$\mathbb{S} = \{ \boldsymbol{s} \in \mathbb{L}_2(V) \} \tag{2.12}$$

In the equation above, the spaces $\mathbb{L}_2$ and $\mathbb{H}^1$ are defined as

$$\mathbb{L}_2 = \left\{ \boldsymbol{v} \Big| \int_V |\boldsymbol{v}|^2 \, \mathrm{d}V < \infty \right\} \tag{2.13}$$

$$\mathbb{H}^1 = \left\{ \boldsymbol{v} \Big| \int_V \left[|\boldsymbol{v}|^2 + |\boldsymbol{v} \otimes \boldsymbol{\nabla}|^2 \right] \mathrm{d}V < \infty \right\} \tag{2.14}$$

The enhanced strain field is computed by

$$\underline{\varepsilon}^{\mathrm{A}} = \underline{\boldsymbol{G}}\underline{\boldsymbol{\alpha}} \tag{2.15}$$

where $\underline{\boldsymbol{G}}$ is an interpolation matrix and where Voigt notation has been used. Two major conditions are put on the enhanced strain field [23]:

- *Condition (i)*. The enhanced strain field and the compatible strain field must be independent. This is reasonable since, if the assumed strain field is to enhance the strain field, the compatible strain field should not be included in $\mathbb{E}$. In addition, it is assumed that the column of $\underline{\boldsymbol{G}}$ are linearly independent.

- *Condition (ii)*. The spaces $\mathbb{S}$ and $\mathbb{E}$ are L_2-orthogonal.

If the second criteria is fulfilled *a priori*, Equation $(2.9)_2$ becomes identically satisfied, and the second term in Equation $(2.9)_1$ vanishes, leading to the reduced set of equations

$$\int_V \delta\boldsymbol{\varepsilon}^A : \boldsymbol{\sigma}^\varepsilon \, \mathrm{d}V = 0 \qquad\qquad \forall \delta\boldsymbol{\varepsilon}^A \in \mathbb{E}$$

$$\int_V \delta\boldsymbol{\varepsilon}^u : \boldsymbol{\sigma}^\varepsilon \, \mathrm{d}V - \int_V \delta\boldsymbol{u} \cdot \boldsymbol{b} \, \mathrm{d}V - \int_\Gamma \delta\boldsymbol{u} \cdot \boldsymbol{t} \, \mathrm{d}V = 0 \qquad\qquad \forall \delta\boldsymbol{u} \in \mathbb{U}^0 \tag{2.16}$$

Note that Equation (2.16) is only dependent on two fields, $\boldsymbol{u}$ and $\boldsymbol{\varepsilon}^{\mathrm{A}}$.

Choosing the interpolation matrix

The Voigt notation for the field variables are henceforth used for the presentation of the EAS-method, i.e

$$\underline{\boldsymbol{\varepsilon}} = \begin{bmatrix} \varepsilon_{\xi\xi} & \varepsilon_{\eta\eta} & \varepsilon_{\zeta\zeta} & \varepsilon_{\xi\eta} & \varepsilon_{\xi\zeta} & \varepsilon_{\eta\zeta} \end{bmatrix}^T \tag{2.17}$$

Furthermore, the ζ-coordinate will denote the thickness direction. The interpolation matrix $\underline{\boldsymbol{G}}$ is evaluated as [23]

$$\underline{\boldsymbol{G}} = \frac{\det\boldsymbol{J}_0}{\det\boldsymbol{J}} \underline{\boldsymbol{T}}_0 \underline{\boldsymbol{M}} \tag{2.18}$$

where $\boldsymbol{J}_0$ and $\boldsymbol{J}$ denotes the Jacobi matrices at the centre of the element and at a Gauss quadrature point, respectively. $\underline{\boldsymbol{T}}_0$ is a transformation matrix for the strain tensor from parent domain to the element coordinate system [18], and is explicitly written as

$$\begin{bmatrix}
j_{11}^2 & j_{12}^2 & j_{13}^2 & 2j_{11}j_{12} & 2j_{11}j_{13} & 2j_{12}j_{13} \\
j_{21}^2 & j_{22}^2 & j_{23}^2 & 2j_{21}j_{22} & 2j_{21}j_{23} & 2j_{22}j_{23} \\
j_{31}^2 & j_{32}^2 & j_{33}^2 & 2j_{31}j_{32} & 2j_{31}j_{33} & 2j_{32}j_{33} \\
j_{11}j_{21} & j_{12}j_{22} & j_{13}j_{23} & j_{11}j_{22}+j_{12}j_{21} & j_{11}j_{23}+j_{13}j_{21} & j_{12}j_{23}+j_{13}j_{22} \\
j_{11}j_{31} & j_{12}j_{32} & j_{13}j_{33} & j_{11}j_{32}+j_{12}j_{31} & j_{11}j_{33}+j_{13}j_{31} & j_{12}j_{33}+j_{13}j_{32} \\
j_{21}j_{31} & j_{22}j_{32} & j_{23}j_{33} & j_{21}j_{32}+j_{22}j_{31} & j_{21}j_{33}+j_{23}j_{31} & j_{22}j_{33}+j_{23}j_{32}
\end{bmatrix} \tag{2.19}$$

where $j_{\alpha\beta}$, $\alpha = \beta = 1, 2, 3$, are the components of the Jacobi matrix. The matrix $\underline{\boldsymbol{M}}$ can be chosen in multiple ways in order to eliminate different locking phenomenas. In [18], the interpolation matrices

in Equation (2.20) and (2.21) are shown to eliminate transverse shear-locking, due to linear and bi-linear enhacement of the transverse shear strains,

$$
\underline{M}^{(1)} = \begin{bmatrix} 0 & 0 & 0 & 0 \\ 0 & 0 & 0 & 0 \\ 0 & 0 & 0 & 0 \\ 0 & 0 & 0 & 0 \\ \xi & 0 & \xi\eta & 0 \\ 0 & \eta & 0 & \xi\eta \end{bmatrix}
\tag{2.20}
$$

$$
\underline{M}^{(2)} = \begin{bmatrix} 0 & 0 & 0 & 0 & 0 & 0 & 0 & 0 \\ 0 & 0 & 0 & 0 & 0 & 0 & 0 & 0 \\ 0 & 0 & 0 & 0 & 0 & 0 & 0 & 0 \\ 0 & 0 & 0 & 0 & 0 & 0 & 0 & 0 \\ \xi & \zeta & 0 & 0 & \xi\zeta & \xi\eta & 0 & 0 \\ 0 & 0 & \eta & \zeta & 0 & 0 & \xi\eta & \eta\zeta \end{bmatrix}
\tag{2.21}
$$

The extension of the linear ζ-terms in Equation (2.21) pays off when the solution for the strain distribution provokes the linear part of the polynomials [18]. Furthermore, to eliminate thickness/Poisson's locking, the normal strain in the thickness direction can be enhanced with, cf. [9]

$$
\varepsilon_{\zeta\zeta}^{A} = \begin{bmatrix} 0 & 0 & 0 & 0 \\ 0 & 0 & 0 & 0 \\ \zeta & \zeta\xi & \zeta\eta & \zeta\eta\xi \\ 0 & 0 & 0 & 0 \\ 0 & 0 & 0 & 0 \\ 0 & 0 & 0 & 0 \end{bmatrix}
\tag{2.22}
$$

In [17], the following matrix was shown to produce good results for membrane and out-of-plane bending analyses

$$
\underline{M}^{(3)} = \begin{bmatrix} \xi & 0 & 0 & 0 & 0 & 0 & 0 & 0 & 0 \\ 0 & \eta & 0 & 0 & 0 & 0 & 0 & 0 & 0 \\ 0 & 0 & \zeta & \xi\zeta & \eta\zeta & \xi\eta\zeta & 0 & 0 & 0 \\ 0 & 0 & 0 & 0 & 0 & 0 & \xi & \eta & \xi\eta \\ 0 & 0 & 0 & 0 & 0 & 0 & 0 & 0 & 0 \\ 0 & 0 & 0 & 0 & 0 & 0 & 0 & 0 & 0 \end{bmatrix}
\tag{2.23}
$$

Since the latter matrix does not enhance the transverse shear strains, shear locking would still exist. Therefore, one can add terms to the transverse shear strains, or use the ANS method; this is described next.

2.5   Assumed Natural Strains

The ANS method was first proposed by Bathe and Dvorkin [5], motivated purely from engineering intuition. The method was later variationaly justified through the Hu-Washizu principle in [13, 14]. The key point in the ANS method, lie in the assumed interpolation of certain strain components. In order to circumvent transverse shear locking, the following interpolation of the compatible transverse shear strains can be used

$$
\varepsilon_{\xi\zeta}^{\text{ANS}} = \frac{1}{2} \left((1 - \eta)\varepsilon_{\xi\zeta}^{A} + (1 + \eta)\varepsilon_{\xi\zeta}^{C} \right)
\tag{2.24}
$$

$$
\varepsilon_{\eta\zeta}^{\text{ANS}} = \frac{1}{2} \left((1 - \xi)\varepsilon_{\eta\zeta}^{D} + (1 + \xi)\varepsilon_{\eta\zeta}^{B} \right)
\tag{2.25}
$$

where $\varepsilon_{\xi\zeta}^{\text{A}}$, $\varepsilon_{\xi\zeta}^{\text{B}}$, $\varepsilon_{\xi\zeta}^{\text{C}}$ and $\varepsilon_{\xi\zeta}^{\text{D}}$ are the transverse shear strains at four sampling points, see Figure 2.2 and Table 2.1.

Furthermore, in order to relieve curvature locking, the following interpolation scheme has proven to be effective, cf. [1]

$$\varepsilon_{\zeta\zeta}^{\text{ANS}} = \frac{1}{4}((1+\xi)(1-\eta)\varepsilon_{\zeta\zeta}^{\text{E}} + (1-\xi)(1-\eta)\varepsilon_{\zeta\zeta}^{\text{F}}+ \tag{2.26}$$

$$(1+\xi)(1+\eta)\varepsilon_{\zeta\zeta}^{\text{G}} + (1-\xi)(1+\eta)\varepsilon_{\zeta\zeta}^{\text{H}}) \tag{2.27}$$

where $\varepsilon_{\zeta\zeta}^{\text{E}}$, $\varepsilon_{\zeta\zeta}^{\text{F}}$, $\varepsilon_{\zeta\zeta}^{\text{G}}$ and $\varepsilon_{\zeta\zeta}^{\text{H}}$ are the transverse shear strains at four sampling points, see Figure 2.2 and Table 2.1.
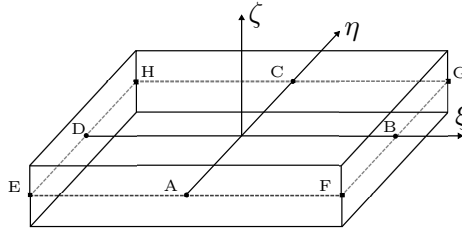
Figure 2.2: *The location of the sampling points A-F used in ANS.*

Table 2.1: Sampling points A-F for ANS method

Point	A	B	C	D	E	F	G	H
(ξ, η)	(0, -1)	(1, 0)	(0, 1)	(-1, 0)	(-1, -1)	(1, -1)	(1, 1)	(-1, 1)

3 Methods for transverse stress prediction in solid-shell elements

As described in the previous sections, predicting the transverse stresses are of particular interest when modeling layered composites, and doing so in an efficient manner. Three approaches in obtaining these stresses is presented in the sections below. The first method is based on enhancing the stress and strain fields with additional degrees of freedom. The second method recovers the transverse stresses in a post-processing step, using the equilibrium equations. The final method, is the straight forward approach of modeling the composite with multiple solid or solid-shell elements through the thickness, thereby obtaining a high resolution of the transverse stresses.

3.1 Enhancement of strains and stresses

By enhancing the eight node solid-shell element with higher order stress and strain fields, the element is given extra flexibility which may improve the transverse stress prediction. The goal of this modeling-technique is to only require one element through the thickness for a layered composite, thereby keeping the computational cost low. This element formulation can therefore be classified as an ESL element. No similar approach can currently not be found in the literature, and is therefore developed in this project.

With the EAS-method (Section 2.4) as a starting point, a variational formulation, with displacements, strains and stresses as independent fields, is developed. The equations in the EAS method contains only two fields, the displacement and assumed strain field. In order to include a higher order variability for the stress field, a third equation is required. The proposed three-field variational formulation is

$$
\int_V \delta\boldsymbol{\varepsilon}^A : \boldsymbol{\sigma}^{\varepsilon}\,\mathrm{d}V = 0 \qquad\qquad \forall\delta\boldsymbol{\varepsilon}^A \in \mathbb{E}
$$

$$
\int_V \delta\boldsymbol{\varepsilon}^u : \boldsymbol{\sigma}\,\mathrm{d}V - \int_V \delta\boldsymbol{u}\cdot\boldsymbol{b}\,\mathrm{d}V - \int_\Gamma \delta\boldsymbol{u}\cdot\boldsymbol{t}\,\mathrm{d}V = 0 \qquad\qquad \forall\delta\boldsymbol{u} \in \mathbb{U}^0 \qquad (3.1)
$$

$$
\int_V (\boldsymbol{\sigma}_{\mathrm{n}} - \boldsymbol{\sigma}_{\mathrm{n}}^{\varepsilon}) : \delta\boldsymbol{\sigma}\,\mathrm{d}V = 0 \qquad\qquad \forall\delta\boldsymbol{\sigma} \in \mathbb{S}
$$

The third equation describes a least squares fit between the transverse stress components $\boldsymbol{\sigma}_n = \{\sigma_{zz} \quad \sigma_{xz} \quad \sigma_{yz}\}$ and the compatible transverse stress components $\boldsymbol{\sigma}_n^{\varepsilon}$. The in-plane stress components, $\boldsymbol{\sigma}_p = \{\sigma_{xx} \quad \sigma_{yy} \quad \sigma_{xy}\}$ are still obtained from the constitutive material relation, i.e $\boldsymbol{\sigma}_p = \boldsymbol{\sigma}_p^{\varepsilon}$. Furthermore, $\boldsymbol{\sigma} = \{\boldsymbol{\sigma}_p \quad \boldsymbol{\sigma}_n\}$ is exchanged for $\boldsymbol{\sigma}^{\varepsilon}$ in Equation $(3.1)_1$ (compare with Equation $(2.16)_1$), to ensure the stress field fulfils equilibrium. Henceforth, subscripts n and m denotes transverse and in-plane components, respectively.

Finite element formulation The discretization of Equation (3.1) is performed as follows. Consider a layered composite with N^{L} layers. The volume integral over an element can then be rewritten as a sum of integrals over each ply

$$
\int_V \bullet\,\mathrm{d}V = \sum_{i=1}^{N^{\mathrm{L}}} \int_{V_i} \bullet\,\mathrm{d}V \qquad (3.2)
$$

In order to avoid performing the FE-formulation in Voigt format, the independent variables, and their corresponding variations, are approximated in tensor form as

$$\boldsymbol{u}(\boldsymbol{x}) = \sum_{i=1}^{N^u} \boldsymbol{N}_i \cdot (\underline{a})_i \qquad \delta\boldsymbol{u}(\boldsymbol{x}) = \sum_{i=1}^{N^u} \boldsymbol{N}_i \cdot (\delta\underline{a})_i$$

$$\varepsilon^A(\boldsymbol{x}) = \sum_{i=1}^{N^\varepsilon} \boldsymbol{G}_i \cdot (\underline{\alpha})_i \qquad \delta\varepsilon^A(\boldsymbol{x}) = \sum_{i=1}^{N^\varepsilon} \boldsymbol{G}_i \cdot (\delta\underline{\alpha})_i \tag{3.3}$$

$$\boldsymbol{\sigma}_n(\boldsymbol{x}) = \sum_{i=1}^{N^\sigma} \boldsymbol{P}_i \cdot (\underline{\beta})_i \qquad \delta\boldsymbol{\sigma}_n(\boldsymbol{x}) = \sum_{i=1}^{N^\sigma} \boldsymbol{P}_i \cdot (\delta\underline{\beta})_i$$

where $\underline{a}$, $\underline{\alpha}$ and $\underline{\beta}$ are vectors containing nodal values, and $(\bullet)_i$ is the i:th component of the vector. Furthermore, $\boldsymbol{N}_i$ are first order tensors consisting of the standard tri-linear shape functions defined in Equation (2.2). $\boldsymbol{G}_i$ are the tensor representation of the interpolation matrix in the EAS method, see Equation (2.18). Finally, $\boldsymbol{P}_i$ are second order tensors defining the interpolation for transverse stress components. In this thesis, $\boldsymbol{\sigma}_\mathrm{p}$ is chosen to vary quadratic within each layer in the element.

From the approximation of the independent variables in Equation (3.3), the compatible stress and strain fields can be computed as

$$\varepsilon^u = [\boldsymbol{\nabla} \otimes \boldsymbol{u}]^\mathrm{sym} = \sum_{i=1}^{N^u} [\boldsymbol{\nabla} \otimes \boldsymbol{N}_i]^\mathrm{sym} \cdot (\underline{a})_i = \sum_{i=1}^{N^u} \boldsymbol{B}_i \cdot (\underline{a})_i$$

$$\boldsymbol{\sigma}^\varepsilon = \mathbf{D} : (\varepsilon^A + \varepsilon^u) = \mathbf{D} : \left(\sum_{i=1}^{N^\alpha} \boldsymbol{G}_i \cdot (\underline{\alpha})_i + \sum_{k=1}^{N^u} \boldsymbol{B}_k \cdot (\underline{a})_k \right) \tag{3.4}$$

where $[\bullet]^\mathrm{sym}$ denotes the symmetric part of the tensor. Inserting Equation (3.4), (3.3) and (3.2) into Equation (3.1), the following equations are obtained,

$$\int_V \delta\varepsilon^A : \boldsymbol{\sigma}^\varepsilon \, \mathrm{d}V = \sum_{i=1}^{N^\varepsilon} (\delta\underline{\alpha})_i \left(\sum_{j=1}^{N^\varepsilon} (\underline{C})_{ij} (\underline{\alpha})_i + \sum_{k=1}^{N^u} (\delta\underline{\alpha})_i (\underline{A})_{ik} (\underline{a})_k \right) = 0 \tag{3.5}$$

$$\int_V \delta\varepsilon^u : \boldsymbol{\sigma} \, \mathrm{d}V = \sum_{i=1}^{N^u} (\delta a)_i \left(\sum_{j=1}^{N^\sigma} (\underline{K})_{ij} (\underline{\beta})_k + \sum_{k=1}^{N^\varepsilon} (\underline{S})_{ik} (\underline{\alpha})_k + \sum_{l=1}^{N^u} (\underline{U})_{il} (\underline{a})_l \right) = \underline{\boldsymbol{F}}^\mathrm{ext} \tag{3.6}$$

$$\int_V (\boldsymbol{\sigma}_n - \boldsymbol{\sigma}_n^\varepsilon) : \delta\boldsymbol{\sigma} \, \mathrm{d}V = \sum_{i=1}^{N^\beta} (\delta\underline{\beta})_i \left(\sum_{j=1}^{N^\beta} (\underline{Q})_{ij} (\underline{\beta})_k - \sum_{k=1}^{N^u} (\underline{R})_{ik} (\underline{a})_k - \sum_{l=1}^{N^\varepsilon} (\underline{L})_{il} (\underline{\alpha})_l \right) = 0 \tag{3.7}$$

where $\underline{\boldsymbol{F}}^\mathrm{ext}$ is the regular external force vector, and where

$$(\underline{C})_{ij} = \int_V \boldsymbol{G}_i : \mathbf{D} : \boldsymbol{G}_j \, \mathrm{d}V, \qquad (\underline{A})_{ik} = \int_V \boldsymbol{G}_i : \mathbf{D} : \boldsymbol{B}_k \, \mathrm{d}V \tag{3.8}$$

$$(\underline{K})_{ij} = \int_V \boldsymbol{B}_i : \boldsymbol{P}_j \, \mathrm{d}V, \qquad (\underline{S})_{ik} = \int_V \boldsymbol{B}_i : \mathbf{D} : \boldsymbol{G}_k^p \, \mathrm{d}V, \qquad (\underline{U})_{il} = \int_V \boldsymbol{B}_i : \mathbf{D} : \boldsymbol{B}_l^p \, \mathrm{d}V \tag{3.9}$$

$$(\underline{Q})_{ij} = \int_V \boldsymbol{P}_i : \boldsymbol{P}_j \, \mathrm{d}V, \qquad (\underline{R})_{ik} = \int_V \boldsymbol{P}_i : \mathbf{D} : \boldsymbol{B}_k^n \, \mathrm{d}V, \qquad (\underline{L})_{il} = \int_V \boldsymbol{P}_i : \mathbf{D} : \boldsymbol{G}_l^n \, \mathrm{d}V \tag{3.10}$$

Using the equations above, the variables $\underline{a}$, $\underline{\alpha}$ and $\underline{\beta}$ can be computed. Since $\underline{\alpha}$ and $\underline{\beta}$ are discontinuous over element boundaries, a static condensation procedure can be performed.

3.2 Stress recovery

As mentioned in the introduction, many elements based on ESL theory are adequate for predicting in-plane stresses, but fails to give reasonable results for the transverse stresses. One way of resolving this, is to utilize stress recovery in a post-processing step. A review of different stress recovery approaches can be found by e.g. Carrera [2] as well as Noor and Malik [16]. In this thesis, the transverses stresses are recovered from the equations of equilibrium (body forces excluded),

$$
\begin{aligned}
\sigma_{xx,x} + \sigma_{xy,y} + \sigma_{xz,z} &= 0 \\
\sigma_{yy,y} + \sigma_{xy,x} + \sigma_{yz,z} &= 0 \\
\sigma_{xz,x} + \sigma_{yz,y} + \sigma_{zz,z} &= 0
\end{aligned}
\tag{3.11}
$$

where $(\bullet)_{,\alpha}$ denotes the derivative with respect to $\alpha = x, y, z$. If the in-plane stress gradients are known, the transverse stress components can be obtained from Equation (3.11) above. Integration from e.g the bottom of the laminate, leads to three expressions

$$
\begin{aligned}
\sigma_{xz} &= -\sum_{n=1}^{N^{\mathrm{L}}} \int_{z^{n-1}}^{z^n} \sigma_{xx,x} + \sigma_{xy,y} \, \mathrm{d}z + C_x \\
\sigma_{yz} &= -\sum_{n=1}^{N^{\mathrm{L}}} \int_{z^{n-1}}^{z^n} \sigma_{yy,y} + \sigma_{xy,x} \, \mathrm{d}z + C_y \\
\sigma_{zz} &= \sum_{n=1}^{N^{\mathrm{L}}} \int_{z^{n-1}}^{z^n} \int_{z^{n-1}}^{z^n} \sigma_{xx,xx} + \sigma_{yy,yy} + 2\sigma_{xy,xy} \, \mathrm{d}z \, \mathrm{d}z + C_{z_1} z + C_{z_2}
\end{aligned}
\tag{3.12}
$$

The equation for the transverse shear stress in Equation $(3.12)_1$ (and Equation $(3.12)_2$), contains one integration constant, C_x, which is determined from the two boundary conditions at the top and the bottom surfaces. This means that only one boundary condition can be enforced. This can be handled by distributing the potential error evenly between the two boundaries, as suggested in [6]. In this work the constant is determined from the bottom boundary (for simplicity).

Due to the fact that the transverse stresses are recovered a posteriori, they become incompatible with the corresponding transverse strain components. In fact, the transverse strains still remain inaccurate. This means that the information obtained from stress-recovery can only be used for predicting damage initiation, and not to describe (for example) material evolution laws, since these laws are generally based on the compatible strains.

The stress recovery in Equation (3.12) is based on the gradients of the in-plane stresses within an element. Unfortunately, the linear displacement assumption in eight node solid elements, limits these stresses to be constant over the element (leading to zero gradient). A method of estimating the gradients of the in-plane stresses are therefore needed. A review of three such methods are presented below.

3.2.1 Least square fit method

One method of obtaining non-zero gradients of the in-plane stresses, is to least square fit a continuous function, say $\boldsymbol{\sigma}^{\mathrm{LSF}}$, to the compatible stress field $\boldsymbol{\sigma}^{\varepsilon}$. This could be performed over all elements in the FE-model, or on local element patches. The mathematical formulation of the least square fit approach can be formulated as,

$$
\boldsymbol{\sigma}^{\mathrm{LSF}} = \arg(\min \Pi), \qquad \Pi = \frac{1}{2} \int_V (\boldsymbol{\sigma}^{\mathrm{LSF}} - \boldsymbol{\sigma}^{\varepsilon}) : (\boldsymbol{\sigma}^{\mathrm{LSF}} - \boldsymbol{\sigma}^{\varepsilon}) \, \mathrm{d}V
\tag{3.13}
$$

The benefits with this approach is that it is simple and straight forward. If the least square fit procedure is performed on specific patches/areas on the model where the transverse stresses are of interest, only a small number of elements needs to be handled, and the method can be considered to be computationally efficient.

3.2.2 Mixed stress-displacement formulation

By using a mixed stress-displacement formulation, the in-plane stresses will be continuous between elements, leading to non-zero gradients. A mixed stress-displacement formulation is derived from the weak form of the equilibrium and constitutive equations, and is presented below

$$\int_V \boldsymbol{\sigma} : \delta\boldsymbol{\varepsilon}^u \, \mathrm{d}V = \int_V \boldsymbol{f} \cdot \delta\boldsymbol{u} \, \mathrm{d}V + \int_S \boldsymbol{t} \cdot \delta\boldsymbol{u} \, \mathrm{d}S \tag{3.14}$$

$$\int_V (\boldsymbol{\varepsilon}^u - \mathbf{D}^{-1} : \boldsymbol{\sigma}) : \delta\boldsymbol{\sigma} dV = 0$$

If the stresses are assumed to vary linearly within each element, the same interpolation and mesh as for the displacement can be used. This means that six additional degree of freedoms, $\sigma_{xx}, \sigma_{yy}, \sigma_{zz}, \sigma_{xy}, \sigma_{xz}$ and σ_{zx}, would be added to each node in the element. This would make it much more computationally expensive compared to standard displacement-based solid elements, but with the added benefit of obtaining continuous stress field without post-processing. Although this approach sounds promising, unwanted effects arises in the results. More specifically, the obtained stress-field is of low quality near boundaries, making it unusable at these areas.

3.2.3 Assuming cylindrical bending

In [22], an estimation of the in-plane stress gradients for an element are obtained by assuming cylindrical plate bending. A brief explanation of the theory is explained below. The equilibrium equations in plate bending relates the moments M with the shear forces T, and can be written as

$$T_{xz} = M_{xx,x} + M_{xy,y} \qquad T_{yz} = M_{yy,y} + M_{xy,x} \tag{3.15}$$

If cylindrical bending is assumed, then $M_{xy,y}$ and $M_{xy,x}$ are zero, and the gradient of the moments can be evaluated from the shear force. Furthermore, the relationship between the strains and sectional forces from classic lamina theory, can be written as,

$$\begin{bmatrix} \underline{N} \\ \underline{M} \end{bmatrix} = \begin{bmatrix} A & B \\ B & D \end{bmatrix} \begin{bmatrix} \varepsilon_0 \\ \kappa \end{bmatrix} \quad \text{giving} \quad \begin{bmatrix} \underline{N}_{,\alpha} \\ \underline{M}_{,\alpha} \end{bmatrix} = \begin{bmatrix} A & B \\ B & D \end{bmatrix} \begin{bmatrix} \varepsilon_{0,\alpha} \\ \kappa_{,\alpha} \end{bmatrix}, \qquad \alpha = x, y \tag{3.16}$$

where the introduced variables may be found in any book describing classical laminate theory. In [22], it is also assumed that the $M_{xx,x}$ and $M_{yy,y}$ are the dominating parts in the force and moment vectors, which leads to the simplification

$$\begin{bmatrix} \underline{N}_{,x} \\ \underline{M}_{,x} \end{bmatrix} = \begin{bmatrix} 0 & 0 & 0 & M_{xx,x} & 0 & 0 \end{bmatrix}^T, \qquad \begin{bmatrix} \underline{N}_{,y} \\ \underline{M}_{,y} \end{bmatrix} = \begin{bmatrix} 0 & 0 & 0 & 0 & M_{yy,y} & 0 \end{bmatrix}^T \tag{3.17}$$

By inverting the ABD-matrix in Equation (3.16), the gradient of the strains can be obtained, which can be inserted into Hooke's law to finally obtain the desired in-plane stress gradients,

$$\underline{\sigma} = \underline{D}\underline{\varepsilon} \qquad \text{giving} \qquad \underline{\sigma}_{,\alpha} = \underline{D}\underline{\varepsilon}_{,\alpha} \tag{3.18}$$

Furthermore, an additional shear correction factor may be needed in order to compensate for the inaccurate shear forces predicted by most shell elements. The shear correction factor is based on the materials and layup for the composite. This approach has demonstrated good results in [22].

3.3 High resolution through the thickness using solid or solid-shell elements

A straight forward approach of modeling layered composites, is to use a large number of solid elements, where one or more solid elements can be used to resolve each laminae in the composite. This means that a high resolution through the thickness of the material is obtained, and the complete stress field can be resolved. The direct disadvantage of this is computationally inefficiency, due to a large number of degree of freedoms.

Traditionally, if this approach is used, the composite structure in question would be modeled with brick-elements. A possible improvement in efficiency would be to use solid-shell elements instead because solid-shell elements allows for a larger aspect ratio for each element without the loss of accuracy. This means that a coarser discretization can be used, with fewer degrees of freedom.

Note that this approach does not qualify as an ESL model, however, can be seen as a simplified LW-model.

4 Numerical examples

In this section, the performance of the solid-shell elements presented in Section 4.1, are assessed and compared. The first two examples investigates the elements abilities to represent the correct displacement for various loading cases. This will give an indication if different locking phenomenas has been eliminated (or if they persist). The remaining examples examines the elements abilities to predict the stress distribution in laminated composites.

4.1 Description of considered solid-shell elements

Using the theory presented in this thesis, various elements are constructed. Two interesting questions to investigate are

1. How different interpolation matrices in the EAS-method (for example Equation (2.20) or (2.21)) and/or in combination with the interpolation from the ANS-method, affects the behaviour of a solid-shell element.

2. The efficiency and performance of the three methods for predicting the transverse stresses, as described in Section 3.

Based on the points above, the following elements are constructed.

Ss8 Standard eight node solid element. This elements is used as a reference to show the improvements obtained with the solid-shell elements.

SS8x A solid-shell element with the stress, strain and displacement as independent field variables, as described in Section 3.1. Quadratic interpolation of the stress-field in each layer is used. The strains are enhanced with the interpolation matrix in Equation (2.20).

SSE1 and SSE2 Solid-shell elements with enhanced strains using the interpolation matrices in Equation (2.20) and (2.21). (Note that these elements will not be used in examples where the stress prediction is of interest. Only the performance in deflection analyses will be investigated).

SSRA3E3 A solid-shell element with ANS interpolation for the transverse shear and normal strains, see Equation (2.24) and Equation (2.26). The remaining strain components are enhanced according to the EAS-matrix in Equation (2.23). The transverse stress components in the material are obtained using the stress recovery approach as described in Section 3.2.

SSsA3E3 The same as *SSRA3E3*, but the stress field is obtained by using multiple elements through the thickness.

The abbreviations of the elements above can be read as follows; *S* (Solid), *SS* (Solid-Shell), *s* (stacked, one or multiple elements through the thickness is used to obtain transverse stresses), *R* (stress recovery used to obtain transverse stresses), *E1* (EAS-method with interpolation matrix 1) and *A1* (ANS-method with interpolation 1).

4.2 Simply supported plate with uniform load

This example investigates the solid-shell elements abilities to predict out-of-plane bending. A simply supported plate subjected to a uniform load is considered, see Figure 4.1a. The aspect ratio of the plate is such that the length to width to height ratio is 100:100:1. The uniformly distributed load, q_0, acts in the negative direction on the top surface. The material used is a unidirectional fibrous composite with transversely isotropic plies, with the following parameters,

$$E_L = 174.6\,\text{GPa}, \quad E_T = 7\,\text{GPa}, \quad G_{LT} = 3.5\,\text{GPa}, \quad G_{TT} = 1.4\,\text{GPa}, \quad \nu_{LT} = 0.25 \qquad (4.1)$$

where subscripts L (x-direction) and T (y-direction) denotes the longitudinal and transverse directions to the fibres, respectively. The deflection at the middle of the plate, $x = L/2, y = L/2$, is studied for different cross-ply layups,

$$[0° \,/\, 90° \,/\, 0°], \quad [0° \,/\, 90° \,/\, 0° \,/\, 90°]_S, \quad [0° \,/\, 90° \,/\, 0° \,/\, 90°]_{2S}$$

Navier's analytical solution is used as a reference [21]. The plate is discretized into 11x11 elements in-plane, and one element out-of-plane. Results from a traditional shell elements using classic laminate plate theory (CLPT) is also presented (which is known to produce good results and is commonly used when analysing composite plate problems).

The deflections for the studied elements are presented in Table 4.1, where it can be seen that all elements produce good results. Element *SSE1* and *SSE2* performs similarly, indicating that the additional EAS-parameters, $\zeta, \eta\xi$ and $\eta\zeta$, used in element *SSE2*, does not contribute to the overall solution. Furthermore, *SSRA3E3* is closest to the analytical solution, and show good agreement with the *CLPT*-element. From this, one can conclude that all major locking phenomenas have been eliminated, in the case of a simply supported plate.

Table 4.1: The deflections, w, and relative error for a simply supported plate with cross-ply layup, predicted by the solid-shell elements.

Layup	$[0° \,/\, 90° \,/\, 0°]$		$[0° \,/\, 90° \,/\, 0°]_S$		$[0° \,/\, 90° \,/\, 0° \,/\, 90°]_{2S}$	
	w	Rel. error (%)	w	Rel. error (%)	w	Rel. error (%)
SS8x	0,9319	2,2500	0,9576	2,6324	0,9589	2,6555
SSE1	0,9319	2,2500	0,9576	2,6324	0,9589	2,6555
SSE2	0,9319	2,2500	0,9576	2,6323	0,9589	2,6555
SSRA3E3	0,9343	2,0012	0,9600	2,3895	0,9613	2,4136
CLPT	0,9343	2,0012	0,9600	2,3880	0,9613	2,4114
Navier (ref.)	0,9534	-	0,9835	-	0,9851	-

4.3 Curved beam with edge load

This example is used to asses the behaviour of solid-shell elements in analyses of curved structures. The dimensions and load of a semi-circular beam can bee seen in Figure 4.1b. The beam consists of a isotropic material with the following Young's modulus and Poisson's ratio

$$E = 10\,\text{MPa}, \quad \nu = 0.25 \qquad (4.2)$$

To asses the convergence rate for the different element types, the vertical tip displacement is analyzed with respect to four different discretizations; 10, 20, 40 and 60 elements (along the beam). An analytical solution for the problem is presented in [12] (0.08734 m), and acts as a reference solution.

The vertical tip displacement, normalized with the reference solution, is plotted in Figure 4.2. Element *SSRA3E3* show good agreement with analytical result, when 40 elements are used. Furthermore, *SSE2* performers better than *SSE1*, where the extra enhancement parameters contributes slightly to the results. These elements does not converge to the analytical solution, indicating that some locking phenomenas are, most likely, still present. One can also note that *SSE1* and *SS8x* produce identical results, since they implement the same EAS-parameters.

(a) *Simply supported plate*

(b) *Curved beam (width = 0.1 m.*
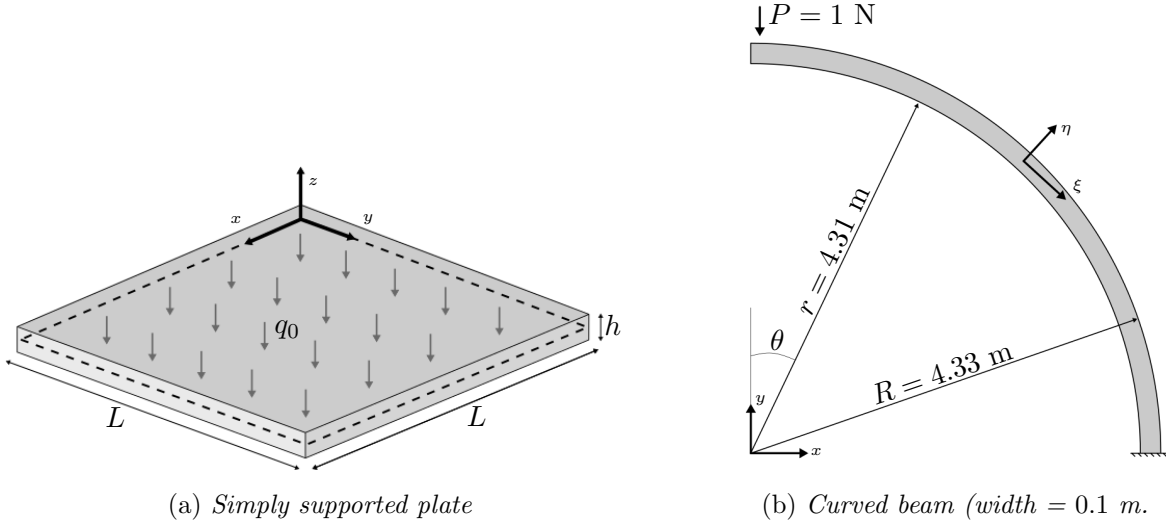
Figure 4.1: *Dimensions and loads defined for the structures in the first two examples.*
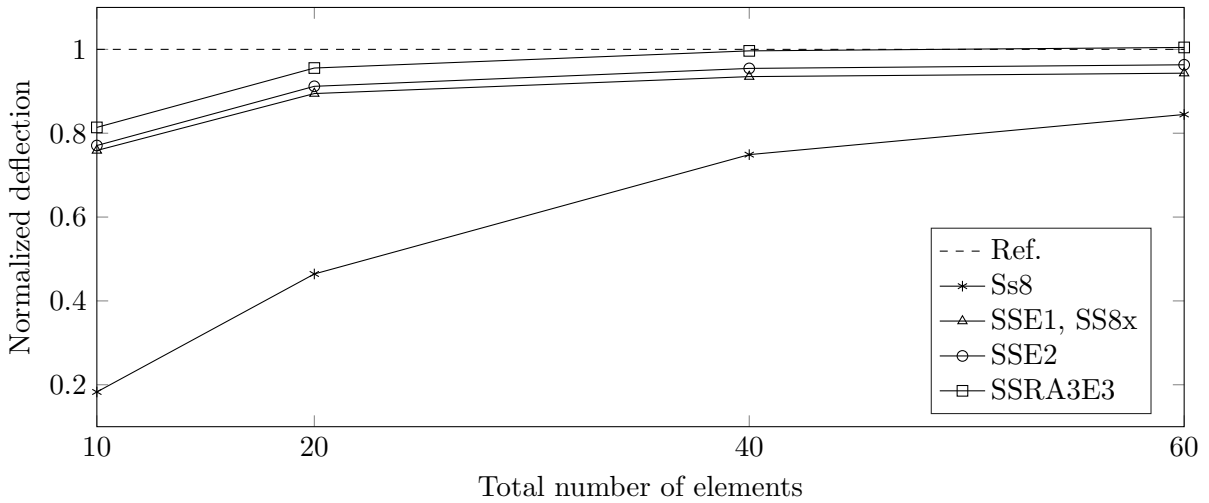
Figure 4.2: *Convergence check for some solid-shell elements in a curved structure. Normalized deflection plotted vs. different dicretizations.*

4.4 Stress prediction in a cantilever beam with uniform load

This example investigates the ability of *SSRA3E3* and *SS8x* to predict the stress state in a thin cantilever beam with a uniformly distributed load, see Figure 4.5a. The beam is analyzed with two materials, one isotropic and one fibrous composite with transversely isotropic material. The isotropic material is mainly used for simple validation against analytical solutions from Euler-Bernoulli beam

theory. The reference solution, for the transversely isotropic material, is a high fidelity mesh with standard solid elements. The aspect ratio of the beam is such that the length to width to thickness ratio is 100:10:1. The beam is discretized using 11 elements along the beam. The three stress components with largest magnitude, σ_{xx}, σ_{xz} and σ_{zz}, at the center of the beam ($x = L/2, y = Z/2$) are considered.

4.4.1 Homogeneous beam

The elastic material is parameters are (Young's modulus, E, and Poisson's ration ,ν)

$$E = 200\,\text{GPa}, \quad \nu = 0.3 \tag{4.3}$$

The resulting stresses can be seen in Figure 4.3. Both elements predicts σ_{xx} and σ_{xz} accurately, however, SS8x is not able to evaluate σ_{zz} in a correct manner.

4.4.2 Laminated beam

The fibrous composite beam consists of a [0° / 90° / 0°] layup, and the material properties defined in Equation (4.1). The stresses predicted by the elements SS8x and SSRA3E3 can be seen in Figure 4.4. Once again, SSRAE3 predicts all stress components accurately, however, element SS8x produces inaccurate results for σ_{xz} and σ_{zz} (σ_{zz} has been scaled by a factor 100, to fit in the plot). Since this element have not been able to accurately predict the transverse stress components, not even for simpler cases, it is not considered in the proceeding studies.
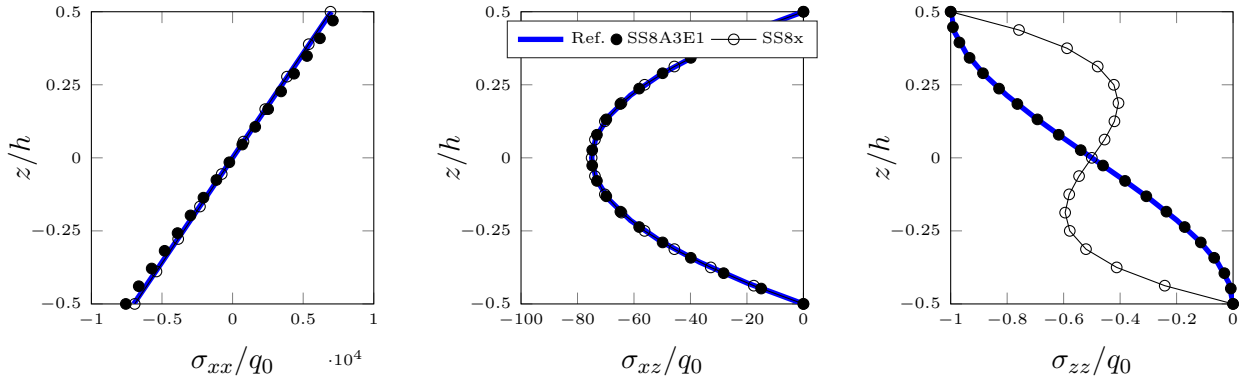
Figure 4.3: *Predicted stresses in a cantilever beam subjected to uniform load with isotropic material.*
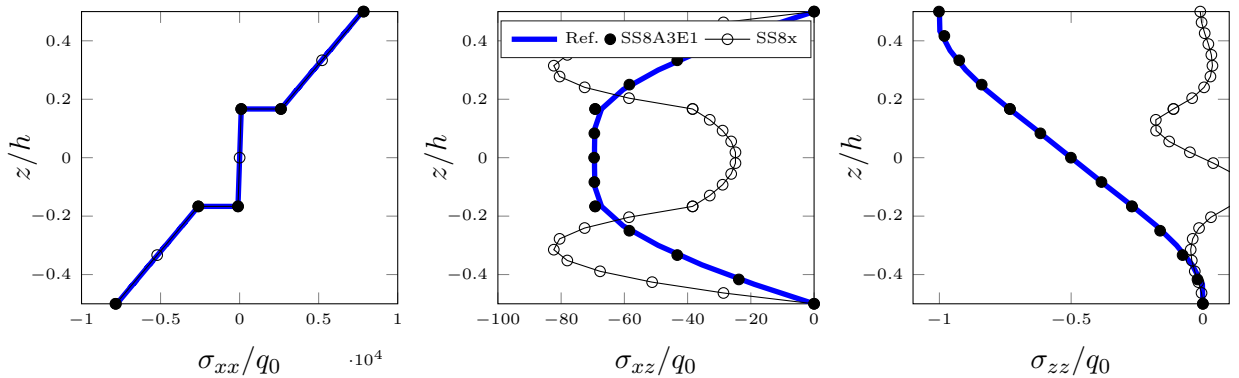
Figure 4.4: *The stresses in a cantilever beam subjected to uniform load with a fibrous composite material with layup [0° / 90° / 0°].*

4.5 Stress prediction in simply supported plate with uniform load

The aim of this example, is to investigate the accuracy of the stresses predicted by *SSRA3E3*, and the possible benefits of using *SSsA3E3* over *Ss8* (i.e stacking of solid-shell or brick elements)

A simply supported plate is considered, with dimension and loads defined in Figure 4.5b. The aspect ratio of the plate is such that the length to width to thickness ratio is 20:20:1. The material is a fibrous composite with transversely isotropic layers, with material parameters defined in Equation (4.1). The layup is [90°/45°/-45°/0°]. As a reference solution, a high fidelity mesh using element *SSsA3E3* is used.

(a) *Cantilever beam.*   (b) *Simply supported plate.*
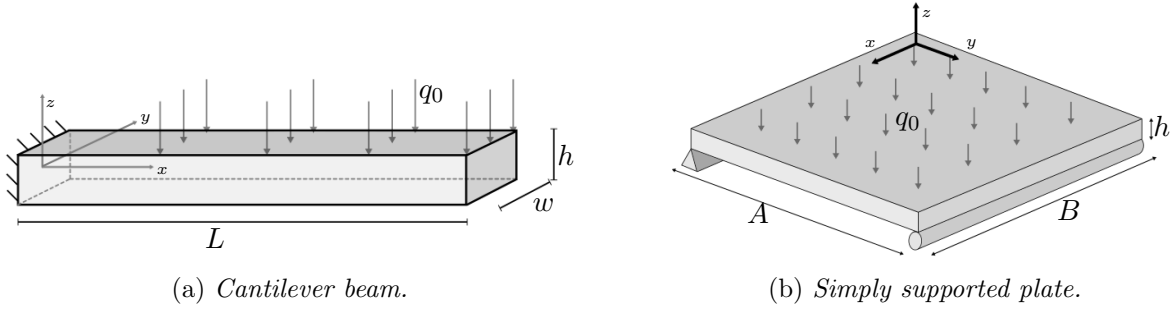
Figure 4.5: *Dimensions for a cantilever beam and simply supported plate.*

Performance of SSRA3E3

The mesh used to asses the performance of *SSRA3E3* is 61 by 61 in-plane, and 1 element in the thickness direction. The stress distribution through the thickness is analyzed at the material point $x = A/4, y = B/4$. The results are presented in Figure 4.6. The element does an excellent job predicting all stress components accurately. Note that only the boundary condition on the bottom surface for σ_{zz} is enforced.
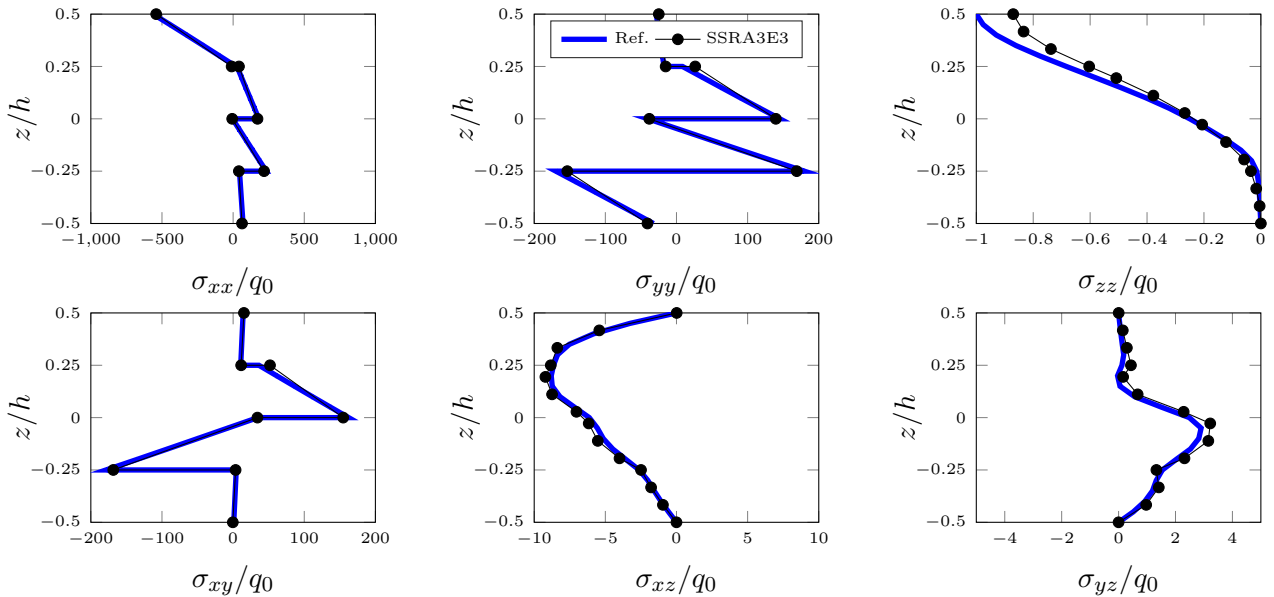
Figure 4.6: *The stress distribution through the thickness predicted by SSRA3E3, in a simply supported plate with layup [90°/45°/-45°/0°].*

Performance benefits with SSsA3E3 over Ss8

Solid-shell elements perform good for larger element aspect-ratios, and the benefits of *SSsA3E3* over *Ss8* is therefore of interest to study. For this reason, the plate is analyzed with three different discretizations, to investigate the structural response for different element aspect ratios. The different mesh sizes used are; 6x6x20, 15x15x20 and 30x30x20 elements in-plane (5 elements per ply).

The maximum deflection, at $x = A/2$ and $y = B/2$, for *Ss8* and *SSsE3A3* is presented in Table 4.2. It can be noted that *Ss8* approaches the reference solution much slower than *SSsE3A3*. The predicted stresses for both elements are presented in Figure 4.7-4.9. The results are summarized as follows:

- *SSsA3E3* accurately predicts the in-plane stresses, even for the coarsest mesh. *Ss8* underestimate the in-plane stresses.

- *SSsA3E3* accurately predicts the deflection for all discretizations, however requires a fine mesh in-plane, to represent the transverse stresses correctly.

- *Ss8* accurately predicts the transverse stresses if a fine mesh is used, even though the maximum deflection has not fully converged.

- *Ss8* appears to oscillate in the prediction of σ_{zz}, which might arise due to thickness locking. *SSsA3E3* eliminates this behaviour from the enhancement of the EAS interpolation, however, this does not affect the average magnitude in the solutions.

Table 4.2: The normalized deflection and relative error predicted by solid-shell elements, for a simply supported plate with composite material. The maximum deflection from the reference solution is $4,2502 \cdot 10^{-6}$ m.

Mesh	6x6x20		15x15x20		30x30x20	
	w [μm]	Rel. error(%)	w [μm]	Rel. error(%)	w [μm]	Rel. error(%)
Ss8	2,1508	49,39588	3,6340	14,49987	4,0696	4,25034
SsA3E3	4,0338	5,09257	4,1716	1,84983	4,2287	0,50769

4.6   Stress distrubution in a curved beam

In this example, we revisit the curved beam in Section 4.3 (see Figure 4.1b). The cross sectional normal stress, $\sigma_{\xi\xi}$, on the inside of the beam is analyzed. The beam is dicretized with 60 elements along the beam, and with 1 element through the thickness. The reference solution is a high fidelity mesh of *Ss8* elements.

The results can be seen in Figure 4.10, where $\sigma_{\xi\xi}$ is plotted against the angle θ. The results are summarized as follows

- *SSRE3A3* predicts a *waviness* in the normal-stress, which is not in agreement with the reference solution. Recall from Section 4.3, that the solution accurately predicts the displacement, and this waviness can therefore not be attributed to a discretization error.

- *SSE2* Shows good agreement with the reference solution (recall from the convergence check in Section 4.3, that *SSE2* has fully converged, but does not approach the reference solution exactly).

From this, it can be concluded that *SSRE3A3* is not a robust element.
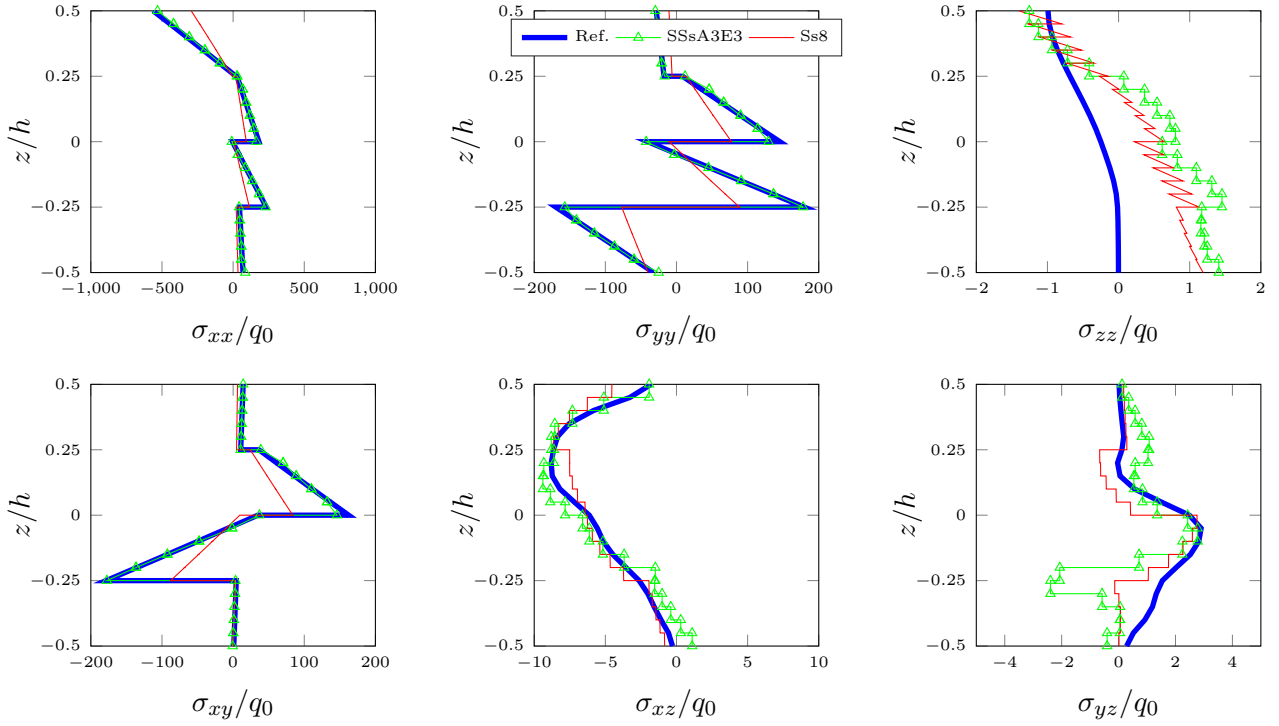
Figure 4.7: *The predicted stresses by Ss8 and SSsA3E3, in a simply supported plate with fibrous composite material with layup [90°/45°/-45°/0°]. The plate is discretized into 6x6x20 elements.*
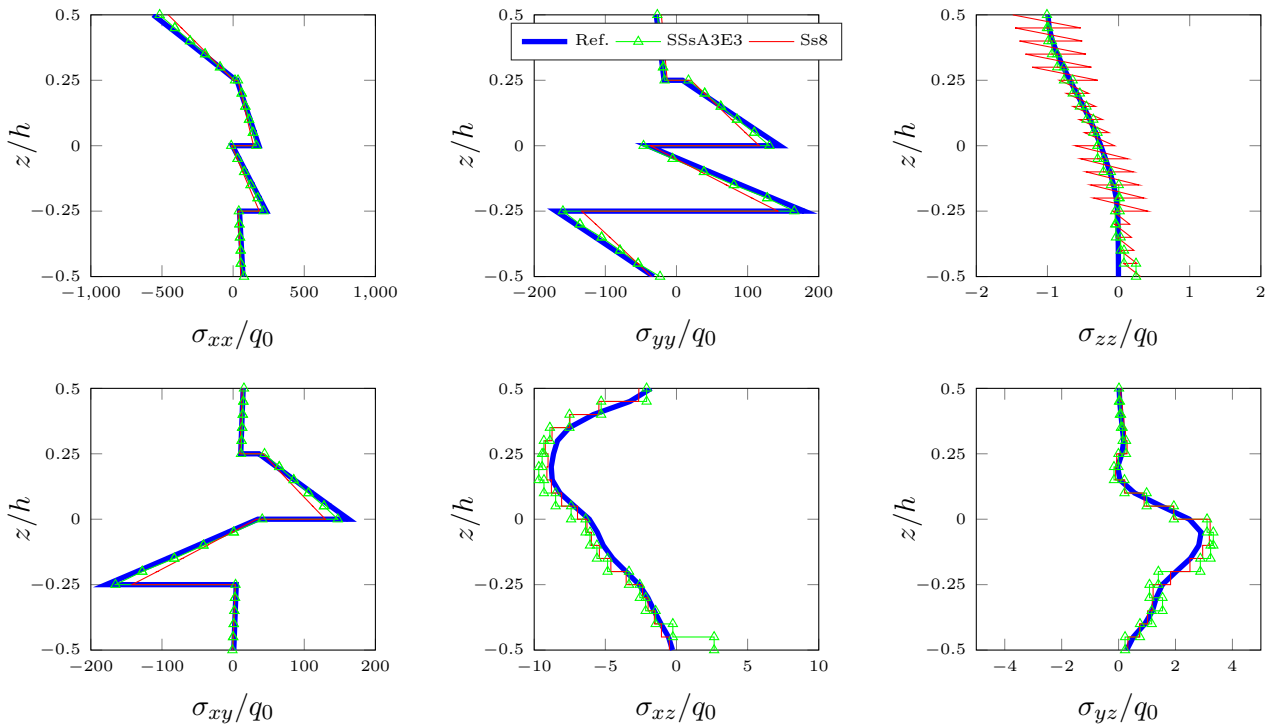
Figure 4.8: *The predicted stresses by Ss8 and SSsA3E3, in a simply supported plate with fibrous composite material with layup [90°/45°/-45°/0°]. The plate is discretized into 15x15x20 elements.*
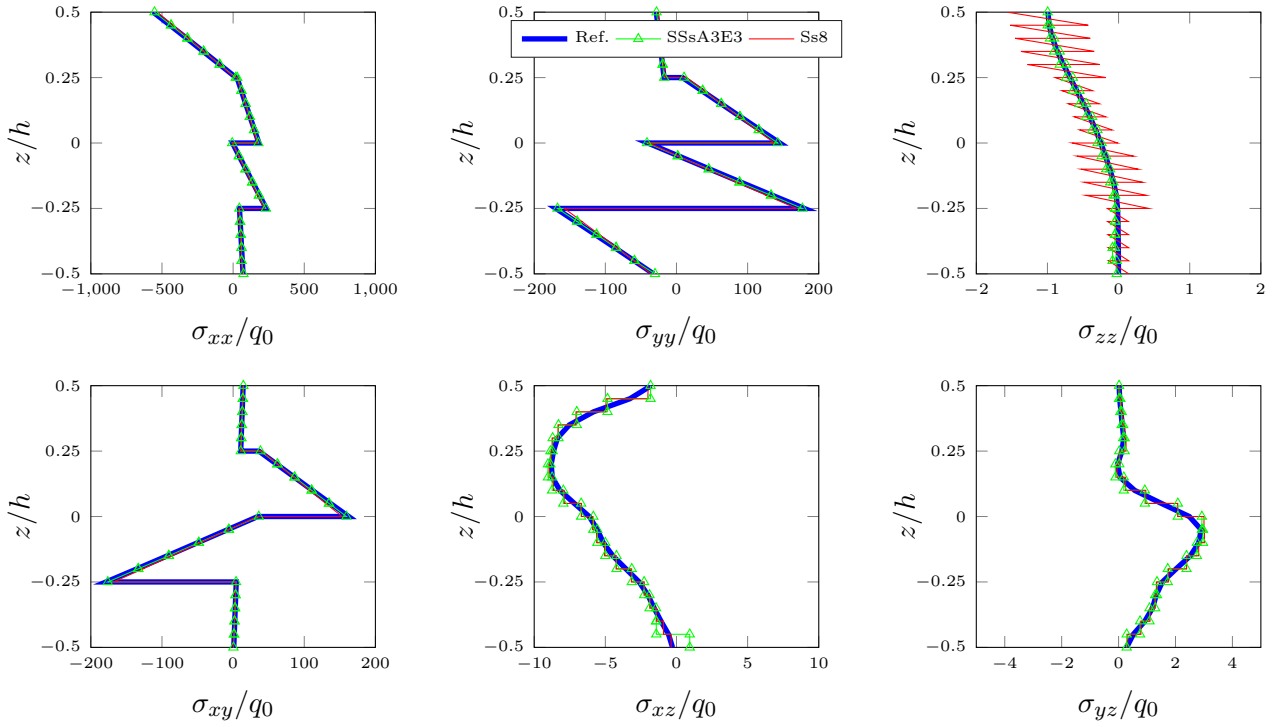
Figure 4.9: *The predicted stresses by Ss8 and SSsA3E3, in a simply supported plate with fibrous composite material with layup [90°/45°/-45°/0°]. The plate is discretized into 30x30x20 element.*
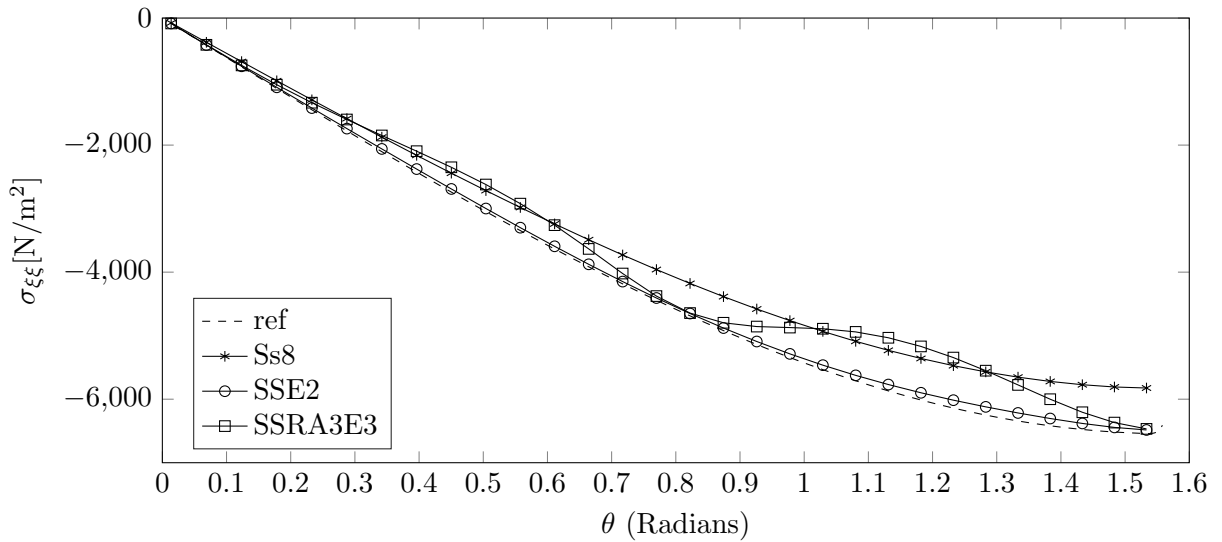
Figure 4.10: *Normal stress $\sigma_{\xi\xi}$ in a curved beam, predicted by different solid/solid-shell elements, with 1 element through the thickness of the beam.*

5   Discussion and conclusions

In this thesis, different solid-shell elements with increased transverse stress predication capabilities have been developed and investigated. The main scope of the thesis was: eliminating locking phenomenas experienced by eight node solid elements and efficiently predicting the transverse stress components in layered composites.

Two method of eliminating the locking-effects was implemented, the enhanced assumed strains (EAS) and assumed natural strains (ANS) methods. The most effective solid-element developed, utilized a combination of the two methods. This element, denoted *SSRA3E3* (and *SSsA3E3*), provided accurate and efficient predictions of the deflections, for planar plate and curved structures (see section 4.1 and 4.3). *SSRA3E3* also predicts the stress distribution in flat beam and plate examples accurately. However, when *SSRA3E3* was used to predict the normal stress in a curved beam, the element performed poorly as shown by a waviness in the stress prediction (see Section 4.6). From this it can be concluded that the element is not very robust. It is still unclear what causes the element to perform poorly. One theory is that the strain field in the element is heavily modified, which might be an advantage for prediction of the deflection, but not for the stresses.

One solid-shell element that performed good in the curved beam stress analysis was *SSE2*. However, from the deflection analyses, it can be seen that the element still exhibit some locking.

SSRA3E3 contains 24 translational degrees of freedom, and 9 internal EAS-parameters; and is therefore slightly more computationally heavy compared to traditional brick elements. The 9 internal parameters can be removed through a static condensation procedure, meaning that implementing the element in a commercial software would be a straight forward task.

Three methods to predict the full 3D stress field of a composite material has been presented. The first method was based on equivalent single layer models, where the stresses and strains was enhanced in hope of obtaining better results. The element using this method, denoted *SS8x*, was shown to give poor results, even for simpler numerical examples. If this type of enhancement-approach is possible, the main challenge is to find a suitable variational formulation with allows for independent variation of the stress, strain and displacement field. The three-field variational formulation developed and used in this thesis, included a least square fit of the compatible stress field, and was the underlying cause behind the inaccurate results. It is unclear if a different formulation would yield better results.

The second approach, also being an equivalent single layer element, recovered the transverse stresses in a post-processing step. This provided very accurate results in an efficient manner. The main challenge in this approach, is to obtain the gradients of the in-plane stresses (which are typically zero in the eight node solid-shell/brick elements). This can be resolved using different techniques, and the one used in this thesis was a simple least square fit of the compatible stresses onto the nodes, on the structural level. This is a relatively efficient approach, and provides sufficient approximations of the in-plane stress gradients.

A second method to approximate the in-plane stress gradients, which has not been investigated in this thesis, is described in [22], and is based on the assumption of cylindrical bending in plates, see Section 3.2.3. The transverse shear stresses are recovered using information about the sectional shear force, without requiring information from the neighboring elements. However, there is often a need for a shear correction factor, to accommodate for the slightly inaccurate shear-stresses predicted by solid and shell elements.

The use of the stress-recovery approach is somewhat limited. The information of the recovered transverse stresses can be used as input to a damage criteria to predict damage initiation, such as delamination. However it is not suitable to use the information for damage evolution or material evolution laws, since these are generally based on the *strains*, which are still inaccurate (in the transverse direction).

The third and last method for better transverse stress prediction, uses multiple solid-shell element

through the thickness of the material. In this thesis, a study of the benefits of using solid-shell elements over standard brick elements was presented. This is discussed in Section 4.5, where it is concluded that solid-shell elements (*SSsA3E3*) can utilize a coarser discretization compared to brick-elements (*Ss8*) when predicting out of plane displacement. Note however, that this approach requires a fine discretization to accurately predict the transverse stresses.

5.1   Outlook

To further analyze the robustness of the solid-shell elements developed, they should be validated against more complex geometries and loading cases. If they are able to produce results that show good agreement with standard shell-elements used today, the solid-shell elements can be considered usable in industrial applications. One weakness of *SSRA3E3* that appeared in the thesis, was the poorly predicted σ_{yy}. Methods of solving this problem needs to be investigate further.

As of now, the stress recovery method is only applied in static problems. In order to incorporate this method in dynamic analyses, for example in crash analyses, further development is needed.

References

[1] P. Betsch and E. Stein. An assumed strain approach avoiding artificial thickness straining for a non-linear 4-node shell element. *Communications in Numerical Methods in Engineering* **11**.11 (1995), 899–909. ISSN: 1099-0887. DOI: 10.1002/cnm.1640111104. URL: http://dx.doi.org/10.1002/cnm.1640111104.

[2] E. Carrera. A priori vs. a posteriori evaluation of transverse stresses in multilayered orthotropic plates. *Composite Structures* **48**.4 (2000), 245–260. ISSN: 0263-8223. DOI: http://dx.doi.org/10.1016/S0263-8223(99)00112-9. URL: http://www.sciencedirect.com/science/article/pii/S0263822399001129.

[3] E. Carrera. Developments, ideas, and evaluations based upon Reissner's Mixed Variational Theorem in the modeling of multilayered plates and shells. *Applied Mechanics Reviews* **54**.4 (2001), 301. ISSN: 00036900. DOI: 10.1115/1.1385512.

[4] J. M. A. César de Sá et al. Development of shear locking-free shell elements using an enhanced assumed strain formulation. *International Journal for Numerical Methods in Engineering* **53**.7 (2002), 1721–1750. ISSN: 1097-0207. DOI: 10.1002/nme.360. URL: http://dx.doi.org/10.1002/nme.360.

[5] E. N. Dvorkin and K.-J. Bathe. A continuum mechanics based four-node shell element for general non-linear analysis. *Engineering Computations* **1**.1 (1984), 77–88. ISSN: 0264-4401. DOI: 10.1108/eb023562.

[6] J. Främby. *On efficient modelling of progressive damage in composite laminates using an equivalent single-layer approach.* 80. Institutionen för tillämpad mekanik, Material- och beräkningsmekanik, Chalmers tekniska högskola, 2016.

[7] Y. Guo, A. P. Nagy, and Z. Gürdal. A layerwise theory for laminated composites in the framework of isogeometric analysis. *Composite Structures* **107** (2014), 447–457. ISSN: 02638223. DOI: 10.1016/j.compstruct.2013.08.016. URL: http://dx.doi.org/10.1016/j.compstruct.2013.08.016.

[8] M. Harnau, R. Hauptmann, and K. Schweizerhof. *On solid-shell elements with linear and quadratic shape functions for small and large deformations.* Institut fur Mechanik, Universität Karlsruhe, 2000.

[9] R. Hauptmann et al. 'Solid-shell' elements with linear and quadratic shape functions at large deformations with nearly incompressible materials. *Computers and Structures* **79**.18 (2001), 1671–1685. ISSN: 00457949. DOI: 10.1016/S0045-7949(01)00103-1.

[10] J. He. Equivalent theorem of Hellinger-Reissner and Hu-Washizu variational principles. *Journal of Shanghai University (English Edition)* **1**.1 (1997), 36–41. ISSN: 1863-236X. DOI: 10.1007/s11741-997-0041-1. URL: http://dx.doi.org/10.1007/s11741-997-0041-1.

[11] Q. Li et al. A new reduced integration solid-shell element based on EAS and ANS with hourglass stabilization. *International Journal for Numerical Methods in Engineering* **104**.8 (2015). nme.4958, 805–826. ISSN: 1097-0207. DOI: 10.1002/nme.4958. URL: http://dx.doi.org/10.1002/nme.4958.

[12] R. H. Macneal and R. L. Harder. A proposed standard set of problems to test finite element accuracy. *Finite Elements in Analysis and Design* **1**.1 (1985), 3–20. ISSN: 0168-874X. DOI: http://dx.doi.org/10.1016/0168-874X(85)90003-4. URL: http://www.sciencedirect.com/science/article/pii/0168874X85900034.

[13] C. Militello and C. A. Felippa. A variational justification of the assumed natural strain formulation of finite elements—I. Variational principles. *Computers and Structures* **34**.3 (1990), 431–438. ISSN: 0045-7949. DOI: http://dx.doi.org/10.1016/0045-7949(90)90267-6. URL: http://www.sciencedirect.com/science/article/pii/0045794990902676.

[14] C. Militello and C. A. Felippa. A variational justification of the assumed natural strain formulation of finite elements—II. The C0 four-node plate element. *Computers and Structures* **34**.3 (1990), 439–444. ISSN: 0045-7949. DOI: http://dx.doi.org/10.1016/0045-7949(90)90268-7. URL: http://www.sciencedirect.com/science/article/pii/0045794990902687.

[15] H. Molker. *Failure prediction of orthotropic Non-Crimp Fabric reinforced composite materials.* Institutionen för tillämpad mekanik, Material- och beräkningsmekanik, Chalmers tekniska högskola, 2016.

[16] K. A. Noor and M. Malik. An assessment of five modeling approaches for thermo-mechanical stress analysis of laminated composite panels. *Computational Mechanics* **25**.1 (2000), 43–58. ISSN: 1432-0924. DOI: 10.1007/s004660050014. URL: http://dx.doi.org/10.1007/s004660050014.

[17] L. Vu-Quoc and X. G. Tan. Optimal solid shells for non-linear analyses of multilayer composites. I. Statics. *Computer Methods in Applied Mechanics and Engineering* **192** (2003), 975–1016. ISSN: 00457825. DOI: 10.1016/S0045-7825(02)00435-8.

[18] N. Quy and a. Matzenmiller. A solid-shell element with enhanced assumed strains for higher order shear deformations in laminates. *Technische Mechanik* (2008), 334–355. URL: http://www.uni-magdeburg.de/ifme/zeitschrift%7B%5C_%7Dtm/2008%7B%5C_%7DHeft3%7B%5C_%7D4/16%7B%5C_%7DMatzenmiller.pdf.

[19] K. Rah, W. Van Paepegem, and J. Degrieck. A novel versatile multilayer hybrid stress solid-shell element. *Computational Mechanics* **51**.6 (2013), 825–841. ISSN: 1432-0924. DOI: 10.1007/s00466-012-0749-z. URL: http://dx.doi.org/10.1007/s00466-012-0749-z.

[20] K. Rah et al. A partial hybrid stress solid-shell element for the analysis of laminated composites. *Computer Methods in Applied Mechanics and Engineering* **200**.49–52 (2011), 3526–3539. ISSN: 0045-7825. DOI: http://dx.doi.org/10.1016/j.cma.2011.08.020. URL: http://www.sciencedirect.com/science/article/pii/S0045782511002751.

[21] J. Reddy. *Mechanics of Laminated Composite Plates and Shells: Theory and Analysis, Second Edition.* Taylor & Francis, 2004. ISBN: 9780203502808. URL: https://books.google.se/books?id=eeUr%5C_AJiGRcC.

[22] R. Rolfes, A. K. Noor, and K. Rohwer. Efficient Calculation of Transverse Stresses in Composite Plates (1997), 1–17.

[23] J. C. Simo and M. S. Rifai. A Class of Mixed Assumed Strain Methods and the Method of Incompatible Modes. *International Journal for Numerical Methods in Engineering* **29**.8 (1990), 1595–1638. DOI: 10.1002/nme.1620290802.